The Canadian Mineralogist
Vol. 48, pp. 81-94 (2010)
DOI: 10.3749/canmin.48.1.81

METAMORPHIC-HYDROTHERMAL REE MINERALS IN THE BACÚCH MAGNETITE DEPOSIT, WESTERN CARPATHIANS, SLOVAKIA: (Sr,S)-RICH MONAZITE-(Ce) AND Nd-DOMINANT HINGGANITE

JAROSLAV PRŠEK§

Department of Mineralogy and Petrology, Faculty of Natural Sciences, Comenius University, Mlynská dolina G, 842 15, Bratislava, Slovakia and AGH University of Science and Technology, Department of Economic and Mining Geology, Al. Mickiewicza 30, 30-059 Kraków, Poland

MARTIN ONDREJKA AND PETER BAČÍK

Department of Mineralogy and Petrology, Faculty of Natural Sciences, Comenius University, Mlynská dolina G, 842 15, Bratislava, Slovakia

BARTOSZ BUDZYŃ

Institute of Geological Sciences, Polish Academy of Sciences, Kraków Research Centre, Senacka 1, 31-002 Kraków, Poland

PAVEL UHER

Department of Mineral Deposits, Faculty of Natural Sciences, Comenius University, Mlynská dolina G, 842 15, Bratislava, Slovakia

ABSTRACT

Accessory REE minerals occur in a small metamorphic magnetite ore deposit at Bacúch, Veporic Superunit, central Slovakia. We distinguish two populations of monazite. Monazite I forms subhedral to euhedral crystals associated with magnetite. It contains ≤12 wt.% ThO_2, ≤2.7% UO_2, ≤0.85% SO_3, with low Ca and Sr contents. Compared to the common monazite-(Ce) I, monazite-(Nd) I (≤26.1% Nd_2O_3) occasionally occurs with an atomic ratio Nd:Ce up to 1.17. Monazite II is present as irregular aggregates with hingganite in younger hydrothermal quartz – albite – chlorite veinlets, or as rim zones on monazite I. Monazite II is depleted in Th and U and has an unusually high content of S (≤11.3% SO_3, 0.31 *apfu* S) and Sr (≤8.7% SrO, 0.18 *apfu* Sr). This composition indicates a $(Ca,Sr)S(REE,Y)_{-1}P_{-1}$ substitution as a dominant mechanism of Sr and S entry into the monazite structure. Some monazite II crystals display an elevated Eu content (≤1.2% Eu_2O_3). Xenotime-(Y) forms subhedral crystals, in association with monazite-(Ce) I, magnetite, pyrite transformed to goethite (?) and quartz. Gadolinite-group minerals at Bacúch are represented by hingganite with an atomic value of $^{X}\square/^{X}(\square + Fe)$ in the range 0.51–0.72. Neodymium is locally the most abundant REE (17.8–18.7% Nd, ~0.56 *apfu*), and an Nd-dominant member of the gadolinite group was identified. The composition of hingganite-(Y) was also determined. The principal mechanism of substitution in hingganite is $Fe^{2+}O_2\square_{-1}(OH)_{-2}$. Primary monazite I and xenotime are most likely products of regional metamorphism, together with magnetite mineralization. On the contrary, Sr- and S-rich monazite II and hingganite originated during a younger (Alpine) metamorphic-hydrothermal overprint in a fluid-rich regime.

Keywords: REE minerals, Sr- and S-rich monazite-(Ce), monazite-(Nd), xenotime-(Y), hingganite-(Y), Nd-dominant hingganite, metamorphic mineralization, Western Carpathians, Slovakia.

SOMMAIRE

Nous signalons la présence de minéraux accessoires de terres rares dans un petit gisement métamorphique de magnétite à Bacúch, superunité de Veporic, en Slovaquie centrale. Nous distinguons deux populations de monazite. La monazite I se présente en cristaux subidiomorphes à idiomorphes associés à la magnétite. Elle contient ≤12% ThO_2, ≤2.7% UO_2, ≤0.85% SO_3 (poids), avec de faibles teneurs en Ca et en Sr. Comparée à la monazite-(Ce) I commune, la monazite-(Nd) I (≤26.1% Nd_2O_3) est localement développée, avec un rapport atomique Nd:Ce jusqu'à 1.17. La monazite II se présente en agrégats irréguliers avec la hingganite dans des veinules hydrothermales tardives de quartz – albite – chlorite, ou bien en surcroissances externes

§ *E-mail address*: prsek@yahoo.com

de monazite I. La monazite II est pauvre en Th et U, et possède une teneur anormalement élevée en S (≤11.3% SO_3, 0.31 *apfu* S) et Sr (≤8.7% SrO, 0.18 *apfu* Sr). Selon cette composition, le schéma de substitution $(Ca,Sr)S(REE,Y)_{-1}P_{-1}$ serait dominant pour expliquer l'incorporation de Sr et de S dans la structure de la monazite. Certains des cristaux de monazite II font preuve de teneurs élevées d'europium (≤1.2% Eu_2O_3). Le xénotime-(Y) forme des cristaux subidiomorphes, en association avec la monazite-(Ce) I, magnétite, pyrite transformée en goethite (?) et quartz. Les minéraux du groupe de la gadolinite sont représentés à Bacúch par la hingganite ayant une valeur atomique de $^{X}\square/^{X}(\square + Fe)$ entre 0.51 et 0.72. Le néodyme est localement la terre rare la plus abondante (17.8–18.7% Nd, ~0.56 *apfu*), et nous identifions un membre du groupe de la gadolinite à dominance de Nd. Nous avons aussi établi la composition de la hingganite-(Y). Le mécanisme principal de substitution dans la hingganite serait $Fe^{2+}O_2\square_{-1}(OH)_{-2}$. La monazite I primaire et le xénotime, ainsi que la minéralisation en magnétite, seraient les produits probables d'un métamorphisme régional. En revanche, la monazite II riche en Sr et en S et la hingganite auraient une origine pendant un événement de circulation d'un fluide métamorphique et hydrothermal plus jeune (alpin).

(Traduit par la Rédaction)

Mots-clés: minéraux de terres rares, monazite-(Ce) riche en Sr et en S, monazite-(Nd), xénotime-(Y), hingganite-(Y), hingganite à dominance de Nd, minéralisation métamorphique, Carpates occidentales, Slovaquie.

Introduction

Monazite, a phosphate mineral of the light rare-earth elements (LREE), is present in a wide range of igneous, metamorphic and sedimentary rocks. Although monazite is usually an accessory mineral, it may control the REE bulk-rock composition because it incorporates large amounts of REE within its structure. Cerium represents the most common cation, and monazite-(Ce) is the most widespread member of the monazite group. Rarely, occurrences of monazite-(Nd), monazite-(La), and monazite-(Sm) have been described (*e.g.,* Graeser & Schwander 1987, Anthony *et al*. 2000, Masau *et al*. 2002). In addition to common Ca, Th and Si admixtures, rare Sr- and S-rich compositions of monazite have also been reported in some magmatic and metamorphic rocks (Kukharenko *et al*. 1961, 1965, Chakhmouradian & Mitchell 1998, 1999, Krenn & Finger 2004, Ondrejka *et al*. 2007, Krenn *et al*. 2008).

The gadolinite group of minerals are relatively rare (Y,REE),Be-bearing silicate phases occurring in some magmatic and metamorphic assemblages. In addition to the most common gadolinite-(Y) and gadolinite-(Ce), octahedral-site-vacant hingganite-(Y), hingganite-(Yb) and hingganite-(Ce) have been described from some granitic–pegmatitic occurrences (*e.g.,* Ding *et al*. 1981, Pezzotta *et al*. 1999, Miyawaki *et al*. 1987, 2007). Some gadolinite–hingganite compositions also show higher Nd contents (up to 8.4 wt.% Nd_2O_3, 0.26 *apfu*: Pezzotta *et al*. 1999); however, the Nd-dominant member has not yet been described.

In this paper, we report the occurrence of monazite-(Ce) unusually enriched in S and Sr, together with S,Sr-poor monazite-(Ce) and monazite-(Nd), and the first natural occurrence of Nd-dominant hingganite in metamorphic, banded and disseminated magnetite mineralization in quartz lenses occurring in the mica schists near Bacúch in the Western Carpathians of central Slovakia. Our detailed electron-microprobe investigation of the monazite and hingganite revealed their compositional variations, principal mechanisms of substitution and possible scenario for their origin and evolution.

Geological Setting

Mineralization in the Bacúch area, Nízke Tatry Mountains, in central Slovakia, is hosted by metamorphosed Paleozoic rocks of the Veporic Superunit (Veporicum) close to the Čertovica fault line. The Veporicum consists mainly of Paleozoic crystalline rocks (Fig. 1) dominated by mica schists, various types of granitic rocks and gneisses, with minor amounts of metavolcanosedimentary and metacarbonate rocks (Biely *et al*. 1992).

The mineralization occurs at Bacúch – Biela Skala, close to Bacúch village, on the eastern slopes of Biela Skala Peak (1250 m a.s.l.). The belt of magnetite-bearing mica schists runs from Beňuš village and Biela Skala to the Javorinka Peak; the most important mine dumps occur between 750 m and 900 m a.s.l. (Fig. 1). The ore samples were collected from the dumps of this ore-lens system at 750 m a.s.l. Lisý (1957) described quartz, chlorite and magnetite. Petro (1973) reported the presence of pyrrhotite, chalcopyrite, sphalerite, hematite and K-feldspar. Both authors noted a massive, banded (quartz and magnetite bands) and disseminated magnetite mineralization in the mica schists. Chovan *et al*. (2000) described monazite, xenotime, zircon, biotite and tourmaline of the dravite–schorl series. J. Pršek (unpublished data) also identified rare cassiterite, native bismuth and bismuth sulfosalts.

Chovan *et al*. (2000) proposed a sedimentary origin for the Fe minerals, affected, however, by younger metamorphism. The Permian age of the magnetite mineralization as a part of the Jánov Grúň volcanosedimentary formation was documented by U–Pb zircon dating of the adjacent metarhyodacites (255 ± 2 Ma: Kotov *et al*. 1996). The Jánov Grúň Formation was later overprinted by Alpine (Cretaceous) low-grade metamorphism, indicated by the Ar–Ar muscovite dating of the adjacent metavolcanic rocks (Dallmeyer *et*

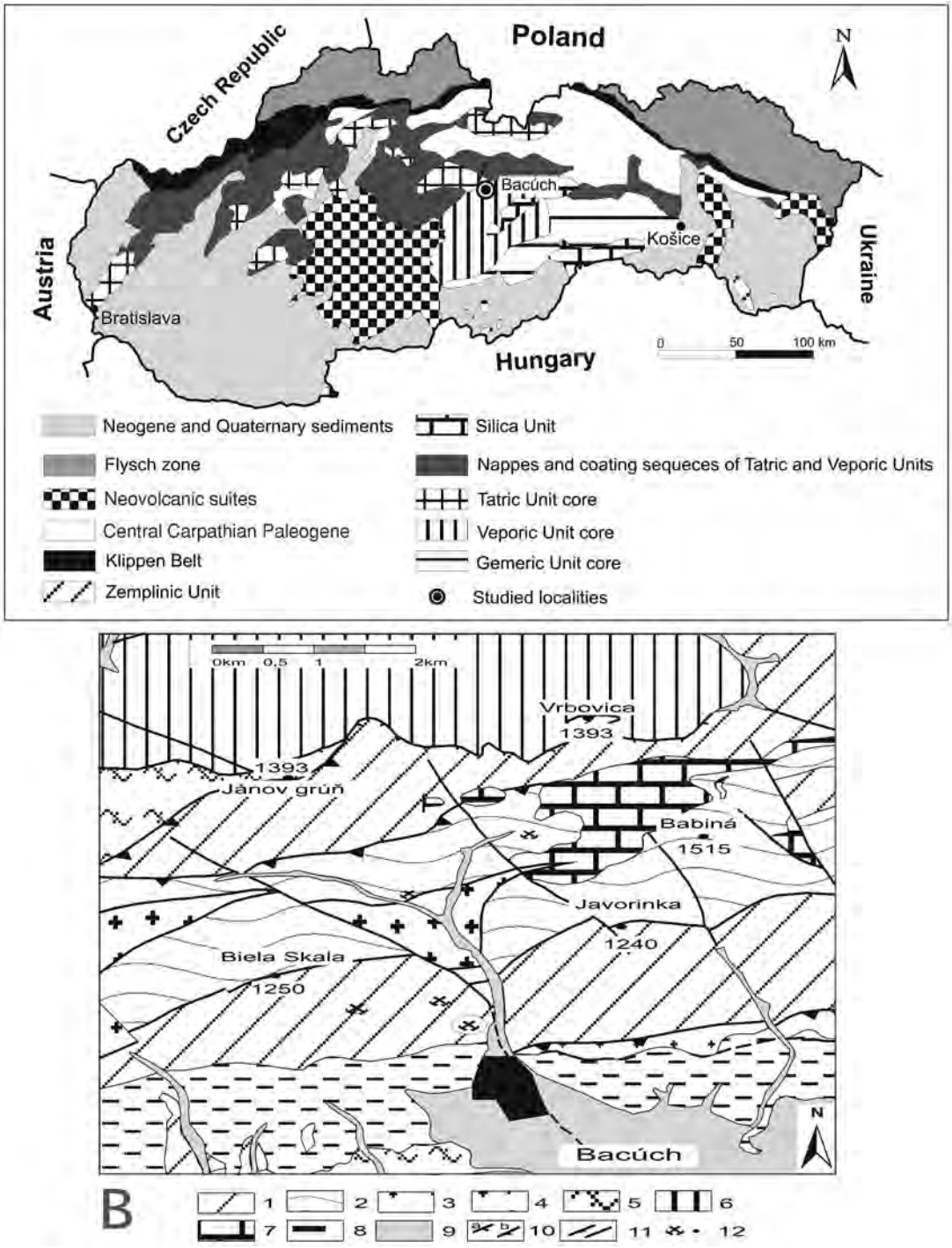

FIG.1. Simplified geological sketch-map of Slovakia (A) and Bacúch surroundings (B) (modified after Biely *et al*. 1992). Symbols: 1–3 Paleozoic metamorphic rocks (Hron complex, Jánov Grúň formation): phyllites micaschists, metarhyolites, 4 Kráľova hoľa complex: granitic rocks, 5 Ľubietová complex: paragneisses, 6 Tatric Unit: granitoids, gneisses, quartzites, limestones, 7 Veľký Bok unit: quartzites, limestones, dolomites, 8 Quaternary, 9 alluvium, 10 nappes lines, a Alpine, b Hercynian, 11 a upthrusts, b faults, 12 mines and dumps.

al. 1993). The P–T conditions of this Alpine overprint was estimated to be 600–700 MPa and 330–350°C, according to phengite geobarometry and mineral association in the adjacent metavolcanosedimentary rocks (Korikovsky *et al*. 1997).

The newest geochronological data on monazite support this Permian and also Alpine events (J. Pršek, unpubl. data).

Experimental Methods

The REE-bearing minerals were analyzed in polished thin sections using Cameca SX–100 electron microprobes at the Dionýz Štúr State Geological Institute (Geological Survey of the Slovak Republic) in Bratislava and at Masaryk University, Brno, Czech Republic. The instruments, operated in wavelength-dispersion (WD) mode, are equipped with four WD spectrometers. The samples were analyzed with LLIF, LPET and standard PET crystals under the following conditions: accelerating voltage 15 kV, sample current 40 nA and a beam diameter of 1–3 μm. The standards utilized, spectral lines, detection limits and standard deviations for the REE elements are presented in Table 1. The matrix effects were corrected using the PAP procedure. Moreover, special care was taken to ensure that line overlaps were properly corrected and also to avoid background interference. Empirically determined correction factors applied to the following line overlaps were used: Th → U, Dy → Eu, Gd → Ho, La → Gd, Ce → Gd, Eu → Er, Gd → Er, Sm → Tm, Dy → Lu, Ho → Lu, Yb → Lu and Dy → As (Konečný *et al*. 2004). Analytical times were 15 to 40 seconds during measurement depending on the expected concentration of the element in the mineral phase. Major elements were measured using shorter times, whereas longer times were applied for elements with low concentrations.

The chemical formula of monazite was calculated on the basis of four oxygen atoms per formula unit (*apfu*). The chemical formula of hingganite was calculated

TABLE 1. CONDITIONS OF ANALYSIS OF THE REE PHASES WITH ELECTRON MICROPROBES

Bratislava			Brno			Both microprobes	
element	line	standards	element	line	standards	detection limits	std. dev.
La	*Lα*	$LaPO_4$	La	*Lα*	LaB_6	0.3 – 0.49	0.08
Ce	*Lα*	$CePO_4$	Ce	*Lα*	$CeAl_2$	0.48 – 0.58	0.09
Pr	*Lβ*	$PrPO_4$	Pr	*Lβ*	PrF_3	0.17 – 0.19	0.13
Nd	*Lβ*	$NdPO_4$	Nd	*Lβ*	NdF_3	0.3 – 0.47	0.12
Sm	*Lβ*	$SmPO_4$	Sm	*Lα*	SmF_3	0.07 – 0.13	0.07
Eu	*Lβ*	$EuPO_4$	Eu	*Lβ*	$EuPO_4$	0.08 – 0.10	0.10
Gd	*Lα*	$GdPO_4$	Gd	*Lβ*	GdF_3	0.11 – 0.12	0.14
Dy	*Lβ*	$DyPO_4$	Dy	*Lα*	$DyPO_4$, DyP_5O_{11}	0.05 – 0.06	0.07
Er	*Lβ*	$ErPO_4$	Er	*Lα*	YErAG	0.05	0.06
Yb	*Lα*	$YbPO_4$	Yb	*Lα*	YbP_5O_{14}	0.09 – 0.10	0.11
Lu	*Lβ*	$LuPO_4$	K	*Kα*	sanidine	0.27 – 0.31	0.37
Tb	*Lα*	$TbPO_4$	Zr	*Lα*	zircon	0.09 – 0.11	0.12
Tm	*Lα*	$TmPO_4$				0.10 – 0.11	0.12
Ho	*Lβ*	$HoPO_4$				0.20 – 0.23	0.24
W	*Lα*	metallic W	Ba	*Lα*	barite		
S	*Kα*	barite	S	*Kα*	barite		
P	*Kα*	apatite	P	*Kα*	apatite-(CaF)		
As	*Lα*	GaAs	As	*Lα*	InAs		
Nb	*Lα*	$LiNbO_3$	Na	*Kα*	albite		
Ta	*Mα*	$LiTaO_3$	Mg	*Kα*	olivine		
Si	*Kα*	wollastonite	Si	*Kα*	spessartine, titanite		
Ca	*Kα*	wollastonite	Ca	*Kα*	cheralite, titanite		
Th	*Mα*	ThO_2	Th	*Mα*	cheralite		
U	*Mβ*	UO_2	U	*Mβ*	UO_2		
Ti	*Kα*	TiO_2	Ti	*Kα*	titanite		
Sn	*Lα*	SnO_2					
Al	*Kα*	Al_2O_3	Al	*Kα*	almandine, sanidine		
Sc	*Kα*	$ScPO_4$	Sc	*Kα*	$ScVO_4$		
Cl	*Kα*	NaCl	Cl	*Kα*	NaCl		
Fe	*Kα*	fayalite	Fe	*Kα*	almandine, andradite		
Mn	*Kα*	rhodonite	Mn	*Kα*	rhodonite		
Pb	*Mα*	PbS	Pb	*Mα*	PbS		
Sr	*Lα*	$SrTiO_3$	Sr	*Lα*	$SrSO_4$		
F	*Kα*	BaF_2	F	*Kα*	topaz		
Y	*Lα*	YPO_4	Y	*Lα*	YAG		

Minerals analyzed at Bratislava: hingganite, monazite, xenotime. Minerals analyzed at Brno: hingganite, monazite. The detection limits and standard deviations are expressed in wt.%.

on the basis of two (S^{6+} + P^{5+} + As^{5+} + Si^{4+} + Al^{3+}) cations per formula unit. The Be^{2+} content was fixed at 2 *apfu*. The content of $(OH)^{-}$ was calculated from the deviation between the ideal anion charges and the sum of the cation charges.

Results

The REE-bearing minerals [monazite-(Ce) I, monazite-(Nd) I, xenotime-(Y), and hingganite-(Y)] are present as individual small crystals or aggregates disseminated in the quartz–magnetite ores in the massive magnetite, or they form a part of younger hydrothermal veinlets [monazite-(Ce) II, hingganite-(Nd)] with albite, chlorite and quartz crossing the magnetite-bearing rocks. The parent rocks consist mainly of magnetite and quartz (Fig. 2A), with minor amounts of chlorite, albite, hematite, cassiterite, ilmenite, tourmaline, pyrite (usually altered to goethite or "limonite"), K-feldspar, muscovite and REE minerals. These minerals usually form disseminated, banded textures, whereas magnetite forming massive ore is less common. Hydrothermal veinlets occasionally consist of quartz, pyrite, hematite, sphalerite, chalcopyrite and Bi sulfosalts cross-cut by magnetite ores.

Monazite and xenotime

Monazite-(Ce) is the most abundant accessory phase and the major LREE carrier in the samples studied. Two populations of monazite were distinguished on the basis of BSE images and chemical composition. Monazite I forms subhedral to euhedral, <200 μm matrix grains that are associated with Fe–Ti oxides, mainly magnetite (Figs. 2B, C, D), and rarely also with xenotime-(Y). Monazite I shows a highly variable Th content (0.0–12.4 wt.% ThO_2, 0.00–0.12 *apfu* Th) and slightly elevated S content (<0.85% SO_3, <0.03 *apfu* S) (Table 2). The Si and Ca contents (<4.1% SiO_2, <0.18 *apfu* Si and 1.3% CaO, 0.06 *apfu* Ca) indicate that Th is primarily incorporated into the monazite I structure according to both huttonite [$ThSi(REE)_{-1}P_{-1}$] and cheralite [$CaTh(REE)_{-2}$] mechanisms of substitution (Fig. 3). Some grains show slightly elevated concentrations of U (<2.7% UO_2, <0.02 *apfu* U) without analogous Si content.

Monazite II is present as irregular aggregates <100 μm in size associated with hingganite in younger hydrothermal quartz–albite–chlorite veinlets (Fig. 2F), or a <10 μm thick rim on monazite I (Figs. 2B, C). The second population is significantly enriched in S (<11.3% SO_3, 0.31 *apfu* S), Sr (<8.7% SrO, 0.18 *apfu* Sr) and depleted in Th (<0.04% ThO_2) (Table 2, Fig. 4). Monazite II compositions show that the elevated S content correlates with Ca and Sr enrichment (up to 0.37 Ca + Sr *apfu*), suggesting a dominant $(Sr,Ca)S(REE,Y)_{-1}P_{-1}$ mechanism of substitution at the expense of the cheralite $CaTh(REE)_{-2}$ substitution (Figs. 3 to 5). The concentration of U is mainly below the detection limit. Very low contents of Th + U are accompanied by systematically elevated amounts of Pb (up to 0.2 wt.% PbO).

Monazite I and monazite II populations differ in their REE and Y distribution. Both populations exhibit a predominance of the LREE, with Ce usually the dominant REE in monazite I (0.32–0.51 *apfu* Ce) and monazite II (0.33–0.48 *apfu* Ce). The Nd content of monazite I, 0.14–0.37 *apfu*, is higher than in monazite II (0.10–0.25 *apfu* Nd). Moreover, the composition of monazite-(Nd) I, with an atomic ratio Nd/Ce of 1.17 (26.1% Nd_2O_3) was occasionally detected (Table 2). Monazite I usually shows higher concentrations of Sm, Eu, Gd and Y, and commonly lower La contents compared to monazite II (Table 2). Chondrite-normalized values of elements such as Sm, Eu, Gd and Tb in monazite I are higher than in monazite II (Fig. 6). The greatest differences were observed in Eu content. Monazite I contains <1.9% Eu_2O_3, whereas monazite II has a lower content, <0.4% Eu_2O_3 (Table 2).

The arsenic concentration in both monazite populations is similar. The atomic As:P ratio is very low, with a maximum value of 0.02, corresponding to 0.5% As_2O_5, which indicates insignificant solid-solution towards gasparite.

Xenotime-(Y) forms subhedral crystals, 30 to 90 μm in size, in association with monazite-(Ce) I, magnetite, pyrite transformed to goethite (?), and quartz (Fig. 2E). Xenotime shows a common composition with strongly dominant Y, HREE >> LREE, and very low S, As, Si, Th, U, Zr and Ca contents.

Hingganite

Minerals of the gadolinite–datolite group in Bacúch are exclusively represented by hingganite, $(Y,REE)_2(\square)Be_2Si_2O_8(OH)_2$. They form anhedral grains 5–30 μm in size and grain aggregates associated with monazite, albite, chlorite and muscovite (Fig. 2F). The $^{X}\square/^{X}(\square + Fe)$ value ranges between 0.51 and 0.72, and the Fe content reaches 0.49 *apfu* (Table 3, Fig. 7). The hingganite is generally Ca-poor, (≤0.01 *apfu*), although a slightly higher content, 0.09–0.13 *apfu* Ca, was also encountered (Table 3, Fig. 6). A majority of analyses reveal a hingganite-(Y) composition with a predominance of Y over other REE. However, some grains display Nd predominance over Y ($1.27 < Nd/Y < 1.41$), suggesting the presence of an Nd-dominant member of the gadolinite group, "hingganite-(Nd)". The Nd concentration attains 17.8–18.7% Nd_2O_3, 0.56–0.57 *apfu* Nd (Table 3, Fig. 8). Concentrations of Y vary between 0.40 and 0.49 *apfu* in "hingganite-(Nd)" and between 0.53 and 1.10 *apfu* in hingganite-(Y), respectively. Contents of the other REE are significantly lower in both hingganite members (Table 3). A

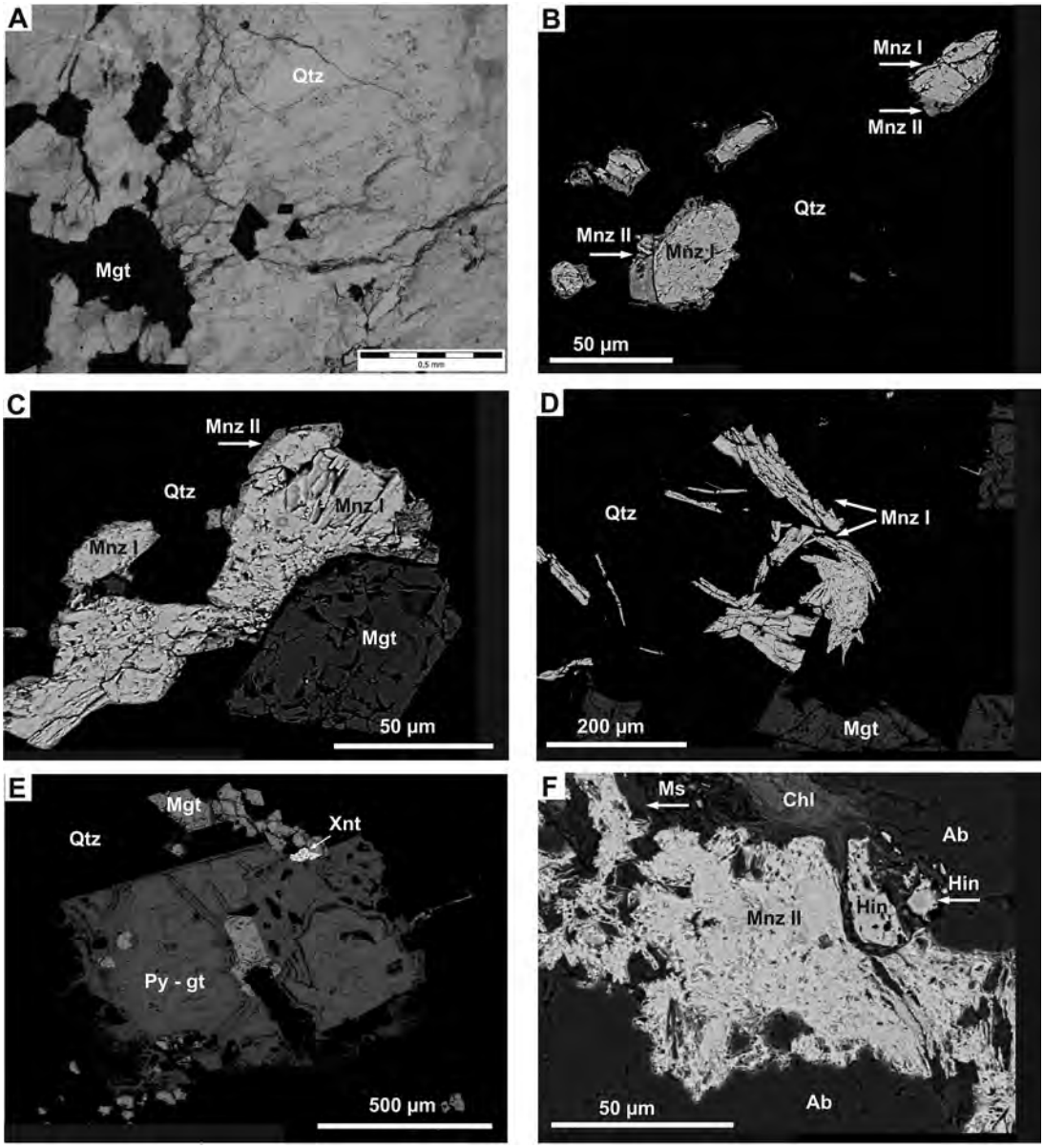

FIG. 2. Microphoto and back-scattered electron (BSE) images of REE accessory minerals from the Bacúch magnetite mineralization. A. Microphoto of quartz (Qtz) – magnetite (Mgt) ore. B. Primary monazite-(Ce), type I (Mnz I) with well-developed (S, Sr)-rich rims of monazite-(Ce), type II (Mnz II) scattered in quartz matrix (Qtz). C. Primary monazite-(Ce), type I (Mnz I) with (S, Sr)-rich rims of monazite-(Ce), type II (Mnz II) in association with magnetite (Mgt) scattered in the quartz matrix (Qtz). D. Aggregate of primary monazite-(Ce), type I (Mnz I) in association with magnetite (Mgt) scattered in the quartz matrix (Qtz). E. Xenotime-(Y) (Xnt) in association with magnetite (Mgt) and pyrite altered to goethite (gt) or limonite scattered in the quartz matrix (Qtz). F. Irregular aggregate of newly formed (S, Sr)-rich monazite-(Ce), type II (Mnz II) in association with hingganite-(Y) and "hingganite-(Nd)" (Hin), chlorite (Chl), muscovite (Ms) and albite (Ab) enclosed in hydrothermal quartz – albite – chlorite veinlets.

TABLE 2. COMPOSITION OF MONAZITE-(Ce) I, MONAZITE-(Nd) I, MONAZITE II AND XENOTIME-(Y) ASSOCIATED WITH THE BACÚCH MAGNETITE MINERALIZATION

Mineral	Mnz-(Ce) I	Mnz-(Ce) I	Mnz-(Ce) I	Mnz-(Nd) I	Mnz-(Ce) II	Mnz-(Ce) II	Mnz-(Ce) II	Mnz-(Ce) II	Mnz-(Ce) II	Mnz-(Ce) II	Mnz-(Ce) II	Mnz-(Ce) II	Xnt
SO_3 wt.%	0.23	0.20	0.29	0.07	10.66	10.36	10.17	8.04	3.44	3.64	7.34	11.12	0.03
P_2O_5	30.20	30.46	31.07	28.86	23.73	23.89	24.03	23.54	26.62	27.56	25.34	22.57	34.78
As_2O_5	0.19	0.16	0.00	0.26	0.11	0.00	0.11	0.11	0.13	0.00	0.00	0.11	0.02
SiO_2	0.22	0.20	0.06	0.12	0.17	0.23	0.18	0.19	0.21	0.07	0.12	1.61	0.14
ThO_2	0.00	0.00	0.00	1.59	0.00	0.00	0.00	0.00	0.00	0.03	0.00	0.00	0.02
UO_2	0.45	2.68	0.00	0.08	0.00	0.00	0.00	0.02	0.00	0.03	0.00	0.00	0.10
Al_2O_3	0.00	0.00	0.00	0.00	0.00	0.03	0.01	0.02	0.00	0.02	0.04	0.01	0.00
Y_2O_3	1.12	0.90	0.35	0.32	0.00	0.00	0.01	0.00	0.05	0.05	0.00	0.01	43.13
La_2O_3	6.75	13.18	14.66	6.09	15.04	13.79	14.90	15.63	17.04	15.96	15.15	12.31	0.00
Ce_2O_3	22.60	24.75	32.42	21.86	27.54	27.70	27.69	28.70	31.95	29.82	29.99	25.76	0.07
Pr_2O_3	4.02	3.38	3.73	4.34	2.88	2.79	2.91	2.72	3.03	3.14	3.00	2.73	0.21
Nd_2O_3	21.92	15.25	14.02	26.12	8.91	8.35	9.30	8.47	9.56	10.83	9.29	9.20	0.23
Sm_2O_3	5.15	2.55	1.77	5.36	0.00	0.79	0.00	0.63	0.77	1.30	0.79	0.95	0.66
Eu_2O_3	1.90	1.63	0.04	1.40	0.10	0.00	0.24	0.10	0.05	0.03	0.00	0.05	1.08
Gd_2O_3	2.69	1.89	0.54	1.85	0.01	0.14	0.00	0.07	0.10	0.26	0.11	0.54	3.17
Tb_2O_3	0.11	0.13	n.a.	0.00	0.10	n.a.	0.01	0.00	0.05	n.a.	n.a.	0.06	0.75
Dy_2O_3	0.54	0.45	0.10	0.14	0.09	0.00	0.00	0.00	0.00	0.04	0.00	0.02	5.60
Ho_2O_3	0.03	0.06	n.a.	0.06	0.00	n.a.	0.03	0.09	0.33	n.a.	n.a.	0.04	1.05
Er_2O_3	0.41	0.24	0.00	0.00	0.43	0.00	0.34	0.00	0.13	0.03	0.00	0.14	3.75
Tm_2O_3	0.22	0.23	n.a.	0.00	0.22	n.a.	0.14	0.00	0.00	n.a.	n.a.	0.10	0.61
Yb_2O_3	0.15	0.07	n.a.	0.10	0.10	n.a.	0.11	0.07	0.09	n.a.	n.a.	0.13	4.24
Lu_2O_3	0.20	0.00	n.a.	0.00	0.20	n.a.	0.11	0.03	0.09	n.a.	n.a.	0.00	0.51
CaO	0.29	0.74	0.41	0.38	4.45	3.97	4.52	4.10	1.97	2.10	3.56	4.95	0.02
SrO	0.01	0.06	0.06	0.08	6.48	7.79	6.25	5.66	3.24	3.17	4.41	8.74	0.00
FeO total	0.79	0.42	0.27	0.10	0.00	0.21	0.00	1.93	0.18	0.33	0.60	0.26	0.96
PbO	0.00	0.03	0.01	0.02	0.05	0.00	0.09	0.15	0.11	0.07	0.08	0.00	0.00
Total	100.20	99.45	99.52	99.10	101.27	100.02	101.18	100.29	99.12	98.48	99.81	101.40	101.14
S^{6+} *apfu*	0.007	0.006	0.008	0.002	0.282	0.276	0.269	0.221	0.100	0.104	0.202	0.290	0.001
P	0.992	1.000	1.010	0.981	0.707	0.718	0.718	0.731	0.870	0.891	0.785	0.664	0.982
As^{5+}	0.004	0.003	0.000	0.005	0.002	0.000	0.002	0.002	0.003	0.000	0.000	0.002	0.000
Si	0.009	0.008	0.002	0.005	0.006	0.008	0.006	0.007	0.008	0.003	0.004	0.056	0.005
Th	0.000	0.000	0.000	0.015	0.000	0.000	0.000	0.000	0.000	0.000	0.000	0.000	0.000
U^{4+}	0.004	0.023	0.000	0.001	0.000	0.000	0.000	0.000	0.000	0.000	0.000	0.000	0.001
Al	0.000	0.000	0.000	0.000	0.000	0.001	0.001	0.001	0.000	0.001	0.002	0.000	0.000
Y	0.023	0.019	0.007	0.007	0.000	0.000	0.000	0.000	0.001	0.001	0.000	0.000	0.766
La	0.097	0.188	0.208	0.090	0.195	0.181	0.194	0.212	0.243	0.225	0.205	0.158	0.000
Ce^{3+}	0.321	0.351	0.455	0.321	0.355	0.360	0.358	0.386	0.452	0.417	0.402	0.328	0.001
Pr	0.057	0.048	0.052	0.064	0.037	0.036	0.038	0.036	0.043	0.044	0.040	0.035	0.003
Nd	0.304	0.211	0.192	0.374	0.112	0.106	0.117	0.111	0.132	0.148	0.121	0.114	0.003
Sm	0.069	0.034	0.023	0.074	0.000	0.010	0.000	0.008	0.010	0.017	0.010	0.011	0.008
Eu	0.025	0.022	0.001	0.019	0.001	0.000	0.003	0.001	0.001	0.000	0.000	0.001	0.012
Gd	0.035	0.024	0.007	0.025	0.000	0.002	0.000	0.001	0.001	0.003	0.001	0.006	0.035
Tb	0.001	0.002	n.a.	0.000	0.001	n.a.	0.000	0.000	0.001	n.a.	n.a.	0.001	0.008
Dy	0.007	0.006	0.001	0.002	0.001	0.000	0.000	0.000	0.000	0.000	0.000	0.000	0.060
Ho	0.000	0.001	n.a.	0.001	0.000	n.a.	0.000	0.001	0.004	n.a.	n.a.	0.000	0.011
Er	0.005	0.003	0.000	0.000	0.005	0.000	0.004	0.000	0.002	0.000	0.000	0.002	0.039
Tm	0.003	0.003	n.a.	0.000	0.002	n.a.	0.002	0.000	0.000	n.a.	n.a.	0.001	0.006
Yb	0.002	0.001	n.a.	0.001	0.001	n.a.	0.001	0.001	0.001	n.a.	n.a.	0.001	0.043
Lu	0.002	0.000	n.a.	0.000	0.002	n.a.	0.001	0.000	0.001	n.a.	n.a.	0.000	0.005
Ca	0.012	0.031	0.017	0.017	0.168	0.151	0.171	0.161	0.081	0.086	0.140	0.184	0.001
Sr	0.000	0.001	0.001	0.002	0.132	0.160	0.128	0.120	0.072	0.070	0.094	0.176	0.000
Fe^{2+}	0.026	0.014	0.009	0.003	0.000	0.006	0.000	0.059	0.006	0.011	0.018	0.008	0.027
Pb	0.000	0.000	0.000	0.000	0.001	0.000	0.001	0.002	0.001	0.001	0.001	0.000	0.000
Total	2.005	1.997	1.994	2.008	2.011	2.015	2.015	2.063	2.031	2.023	2.025	2.036	2.017
A site	0.993	0.981	0.974	1.015	1.014	1.013	1.019	1.101	1.051	1.025	1.033	1.025	1.029
X site	1.012	1.016	1.020	0.993	0.997	1.002	0.996	0.962	0.980	0.998	0.991	1.011	0.988

Formulae based on four atoms of oxygen; n.a.: not analyzed.

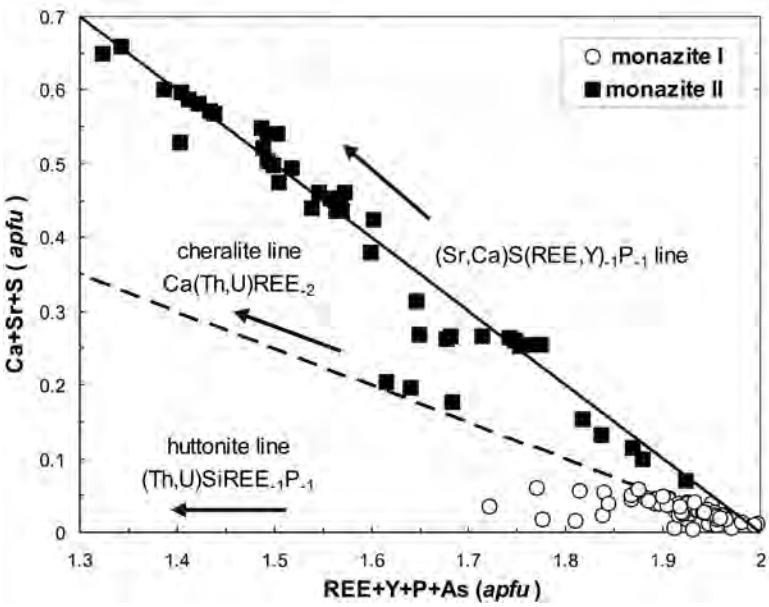

FIG. 3. Composition of monazite-(Ce) from the Bacúch magnetite mineralization in plot of Ca + Sr + S *versus* REE + Y + (P + As) normalized to 2 *apfu*, with ideal cheralite $Ca(Th,U)REE_{-2}$ (dashed line) and $(Ca, Sr)S(REE,Y)_{-1}(P,As)_{-1}$ substitution vectors (solid line).

TABLE 3. COMPOSITIONS OF HINGGANITE ASSOCIATED WITH THE BACÚCH MAGNETITE MINERALIZATION

Mineral	hin-(Y)	hin-(Y)	hin-(Y)	hin-(Nd)	hin-(Nd)	hin-(Nd)	Mineral	hin-(Y)	hin-(Y)	hin-(Y)	hin-(Nd)	hin-(Nd)	hin-(Nd)
P_2O_5 wt.%	0.02	0.03	0.18	0.00	0.00	0.03	P *apfu*	0.001	0.002	0.012	0.000	0.000	0.002
As_2O_5	n.a.	0.12	0.01	n.a.	n.a.	0.20	As^{5+}	n.a.	0.005	0.002	n.a.	n.a.	0.009
SiO_2	24.08	23.70	24.33	22.68	22.92	23.48	Si	1.999	1.993	1.972	2.000	2.000	1.989
UO_2	0.03	0.01	0.08	0.06	0.06	0.00	Al	0.000	0.000	0.014	0.000	0.000	0.000
Al_2O_3	0.00	0.00	0.13	0.00	0.00	0.00	*T* site	2.000	2.000	2.000	2.000	2.000	2.000
Y_2O_3	12.19	11.78	25.81	9.22	8.63	9.83							
La_2O_3	2.39	0.84	0.15	1.17	1.16	1.03	Be + B	2.000	2.000	2.000	2.000	2.000	2.000
Ce_2O_3	11.61	7.33	1.94	8.75	9.04	8.26							
Pr_2O_3	2.55	2.39	0.69	2.54	2.51	2.45	Fe^{2+}	0.276	0.420	0.392	0.420	0.438	0.486
Nd_2O_3	14.05	16.23	3.83	17.83	18.16	18.65	$^{X}\square$	0.724	0.580	0.608	0.580	0.561	0.514
Sm_2O_3	4.59	6.95	2.66	7.77	7.85	7.25							
Eu_2O_3	n.a.	2.06	1.30	n.a.	n.a.	1.90	U^{4+}	0.001	0.000	0.001	0.001	0.001	0.000
Gd_2O_3	3.79	5.19	3.98	5.04	5.00	4.22	Y	0.538	0.527	1.113	0.433	0.401	0.443
Tb_2O_3	n.a.	0.55	0.81	n.a.	n.a.	0.35	La	0.073	0.026	0.004	0.038	0.037	0.032
Dy_2O_3	2.40	2.46	5.21	2.26	2.07	1.73	Ce^{3+}	0.353	0.226	0.058	0.282	0.289	0.256
Ho_2O_3	n.a.	0.46	0.80	n.a.	n.a.	0.33	Pr	0.077	0.073	0.020	0.081	0.080	0.076
Er_2O_3	0.74	0.96	2.33	0.55	0.55	0.85	Nd	0.417	0.487	0.111	0.561	0.566	0.564
Tm_2O_3	n.a.	0.21	0.39	n.a.	n.a.	0.22	Sm	0.131	0.201	0.074	0.236	0.236	0.212
Yb_2O_3	0.52	0.77	1.26	0.61	0.50	0.66	Eu	n.a.	0.059	0.036	n.a.	n.a.	0.055
Lu_2O_3	n.a.	0.12	0.23	n.a.	n.a.	0.25	Gd	0.104	0.145	0.107	0.147	0.145	0.118
CaO	1.05	0.02	1.55	0.02	0.00	0.03	Tb	n.a.	0.015	0.022	n.a.	n.a.	0.010
SrO	0.01	0.02	0.02	0.00	0.00	0.02	Dy	0.064	0.067	0.136	0.064	0.058	0.047
FeO total	3.97	5.98	5.79	5.70	6.01	6.85	Ho	n.a.	0.012	0.021	n.a.	n.a.	0.009
BeO*	10.03	9.90	10.27	9.44	9.54	9.83	Er	0.019	0.025	0.059	0.015	0.015	0.023
H_2O**	3.40	2.62	2.79	2.59	2.75	2.45	Tm	n.a.	0.005	0.010	n.a.	n.a.	0.006
							Yb	0.013	0.020	0.031	0.017	0.013	0.017
Total	97.41	100.70	96.54	96.21	96.74	100.88	Lu	n.a.	0.003	0.006	n.a.	n.a.	0.007
							Ca	0.094	0.002	0.134	0.001	0.000	0.003
							Sr	0.001	0.001	0.001	0.000	0.000	0.001
							W site	1.885	1.895	1.945	1.877	1.840	1.878
							REE – Y	1.252	1.365	0.695	1.442	1.439	1.431
							Σ cations	6.162	6.316	6.338	6.299	6.279	6.365
							O^{2-}	9.059	9.266	9.247	9.239	9.200	9.308
							OH^-	1.883	1.467	1.507	1.521	1.600	1.385
							Me/Si***	0.943	0.951	0.986	0.939	0.920	0.944

The formulae are based on (S + P + As + Si + Al) = 2 atoms, Be = 2 atoms per formula unit (*apfu*). * Calculated from ideal stoichiometry (Be^{2+} + B^{3+} = 2 *apfu*). ** Calculated from deviation of sum of cation charges from ideal sum of O^{2-} charge = 10. *** Ratio (atomic) of the metals in the *W* site to Si.

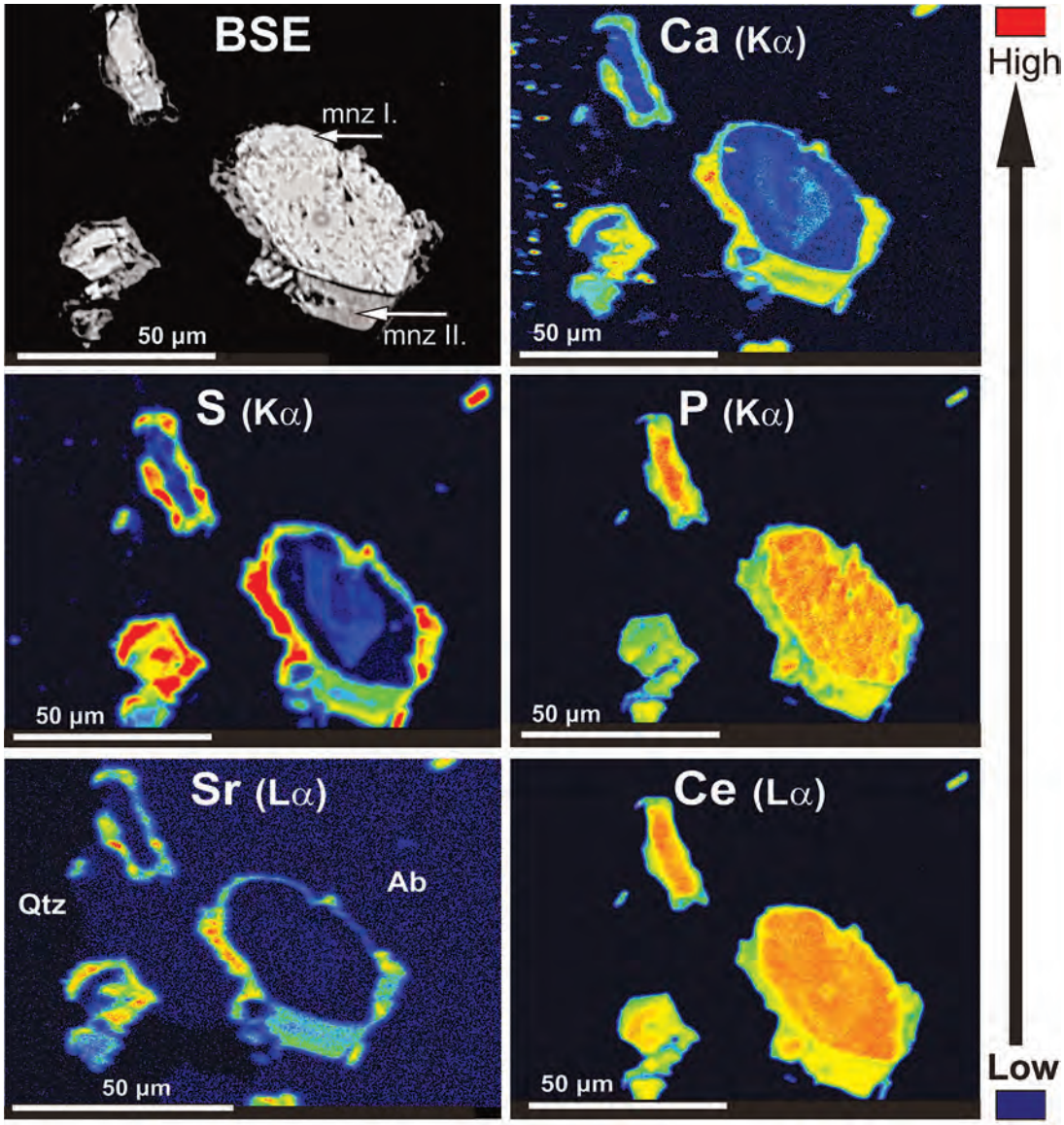

FIG. 4. BSE image and corresponding X-ray compositional maps of Ca, S, P, Sr and Ce for monazite I (mnz I) and monazite II (mnz II). Maps show relative enrichment of S, Sr, Ca and depletion of P, Ce in monazite II. The inverse trend is observed for monazite I.

normalized plot of the REE generally shows an almost flat pattern, with increase from La to the middle REE and a subsequent slight decrease to Lu (Fig. 6). The content of other elements, such as U, Ti, Al, Mn and Mg, is very low or below the detection limit of the electron microprobe. The composition of the Bacúch hingganite is mainly controlled by the gadolinite-type substitution $[Fe^{2+}O_2\square_{-1}(OH)_{-2}]$, whereas a datolite-type substitution, along the $CaB(Y,REE)_{-1}Be_{-1}$ vector, is very restricted owing to a low Ca content in hingganite (<0.13 *apfu*, Table 3, Fig. 7).

DISCUSSION

Monazite-(Ce) represents the dominant LREE phosphate phase of the Bacúch magnetite ore assem-

blage (Fig. 2). Primary accessory monazite-(Ce) I to monazite-(Nd) I forms large subhedral to euhedral crystals with a chemical composition close to the ideal $LREEPO_4$ end member, with a high Th content in some areas defining a monazite – cheralite – huttonite solid solution (*e.g.*, Bea 1996, Förster 1998). A second generation usually forms anhedral and fine-grained irregular monazite-(Ce) II aggregates or recrystallized rims on the primary monazite I. An analogous form of secondary monazite of hydrothermal origin was also documented by Schandl & Gorton (2004), Krenn & Finger (2007), and Zych-Habel *et al*. (2007).

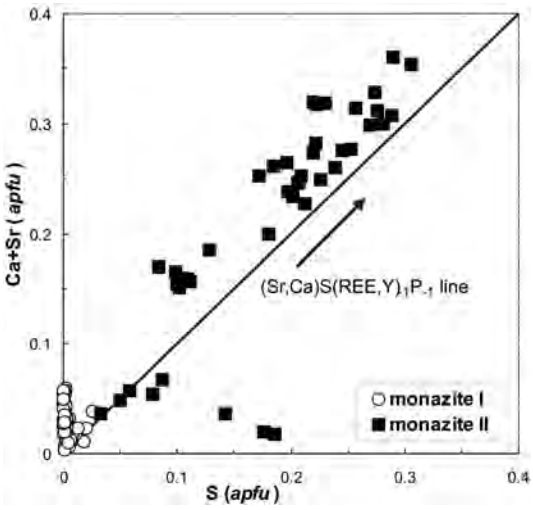

FIG. 5. Composition of monazite-(Ce) from the Bacúch magnetite mineralization in Ca+Sr *versus* S correlation diagram normalized to 2 *apfu*. The straight line represents the ideal 1:1 ratio in $(Ca,Sr)SO_4$.

The variation in monazite composition is driven by isomorphous chemical substitutions. The simplest one involves the replacement of one REE^{3+} (or Y^{3+}) cation by another REE^{3+} (or Y^{3+}) cation. The larger, nine-fold-coordinated LREE cations are more favorably incorporated into the monoclinic structure of monazite than in the smaller, eight-fold-coordinated site well suited for the heavy rare-earth elements and Y (HREE + Y), which are dominant in the tetragonal structure of xenotime (Ni *et al*. 1995). The enrichment in Nd or La was explained in relationship to the formation of monazite in a strongly oxidizing environment and high pH, causing the hydrolysis of Ce^{4+} and subsequent removal of most of the Ce from the solution (Demartin *et al*. 1991). Consequently, the presence of Nd-rich monazite-(Ce) I to monazite-(Nd) I in association with magnetite at Bacúch indicates a high fugacity of oxygen during its precipitation. In addition, the elevated Eu content in monazite I (<1.9% Eu_2O_3) and the lack of a negative Eu anomaly in chondrite-normalized patterns (Fig. 5) may reflect the presence of Eu^{3+}, which can enter the structure more easily than the larger Eu^{2+}. This possibly points to monazite crystallization under high fugacity of oxygen (Krenn *et al*. 2008).

The monazite II from Bacúch reveals the highest S and Sr contents reported in nature (<11.3% SO_3, <0.31

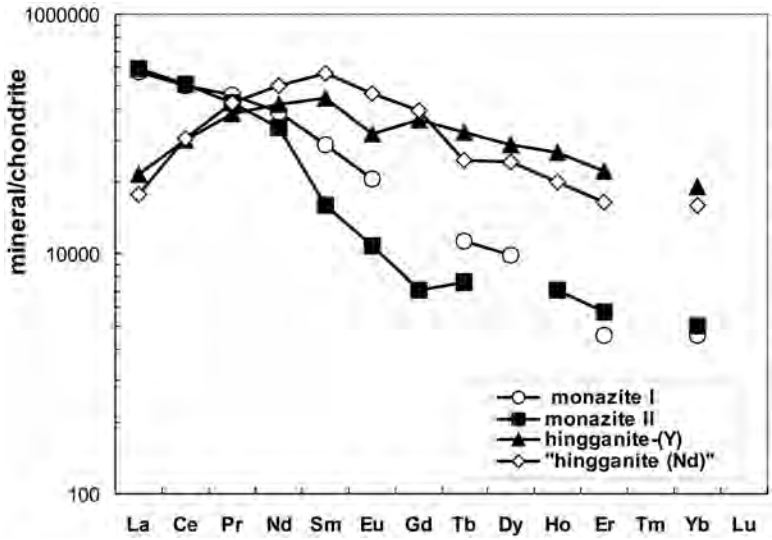

FIG. 6. Average chondrite-normalized REE patterns of monazite-(Ce) from the Bacúch magnetite mineralization. Chondrite values from Taylor & McLennan (1985).

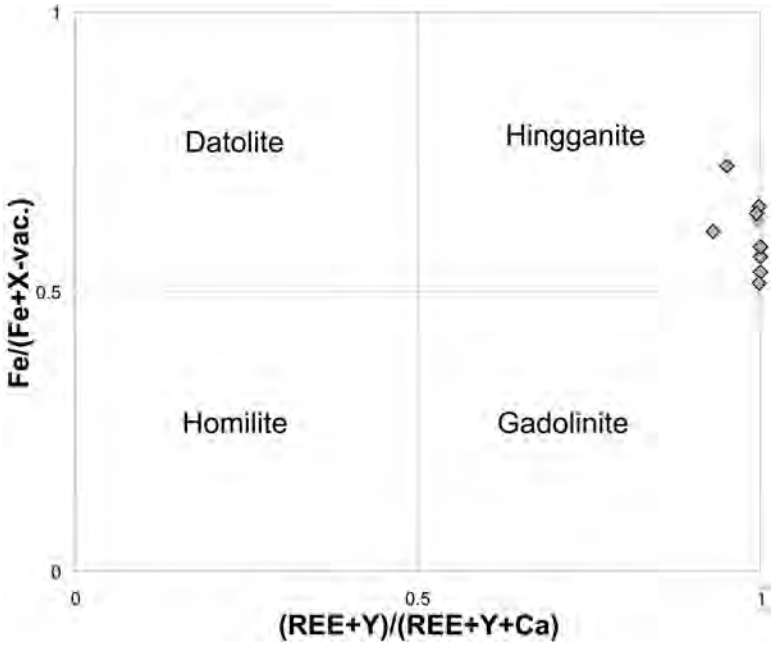

FIG. 7. Classification plot of the gadolinite-group minerals $^{X}\square/{}^{X}(\square + Fe)$ *versus* $^{W}(Y + REE)/{}^{W}(Y + REE + Ca)$.

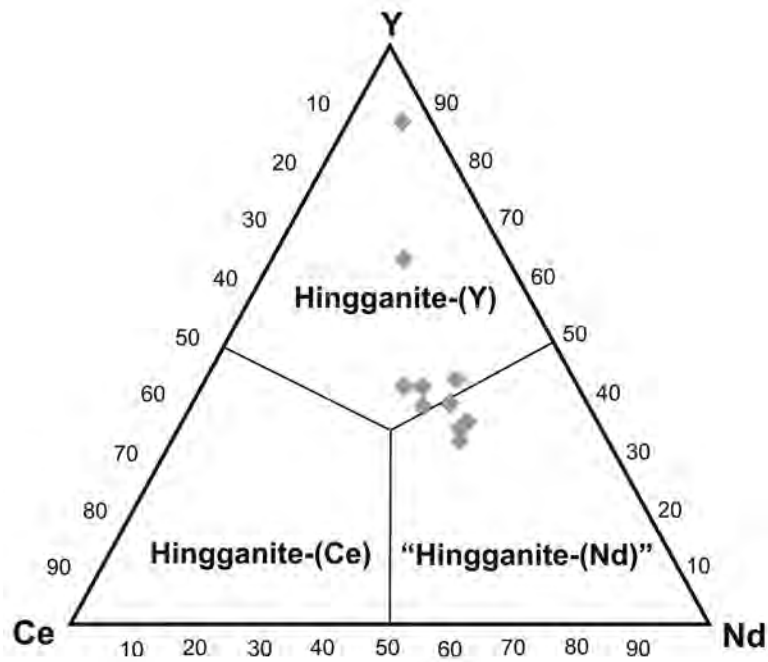

FIG. 8. Triangular Y – Ce – Nd plot showing the occupants at the *W* site in hingganite.

apfu S; Sr <8.7% SrO, 0.18 *apfu* Sr). Sulfur shows a positive correlation with Ca + Sr (Fig. 5), but does not correlate with Si content. There is also negligible Th content (Table 1, Fig. 4). Therefore, the substitution $(Ca,Sr)S(REE,Y)_{-1}P_{-1}$ or $(Ca,Sr)^{2+} + (SO_4)^{2-} \leftrightarrow (REE,Y)^{3+} + (PO_4)^{3-}$ is interpreted as the dominant mechanism (Fig. 3). The synthesis of a monoclinic, monazite-type $CaSO_4$ polymorph ("clinoanhydrite") at 2 to 28 GPa and room temperature (Borg & Smith 1975, Crichton *et al*. 2005, Bradbury & Williams 2009) indicates the possibility of incorporating $CaSO_4$ within the monazite structure in significant amounts. The role of $SrTh(REE,Y)_{-2}$ (Chakhmouradian & Mitchell 1998) or $SiSP_{-2}$ (Cressey *et al*. 1999, Jercinovic & Williams 2005) substitutions is negligible owing to very low Si and Th contents in the monazite II at Bacúch. Elevated contents of S and Sr in natural monazite (<8.5% SO_3 and up to <8.3% SrO) and the $(Ca,Sr)S(REE,Y)_{-1}P_{-1}$ mechanism of substitution have only been reported from a few localities, including carbonatite occurrences in the Kola Peninsula, Russia (Kukharenko *et al*. 1961, 1965, Chakhmouradian & Mitchell 1998), calcite kimberlite from Internatsional'naya, Yakutia (Chakhmouradian & Mitchell 1999), garnet-rich high-pressure rocks from the Bohemian Massif (Krenn & Finger 2004), A-type rhyolite from Tisovec–Rejkovo, Slovakia (Ondrejka *et al*. 2007), and ore-bearing mylonitic mica schists and aplitic material from the Schellgaden mining district in Austria (Krenn *et al*. 2008). The precipitation of such anomalously S- and Ca(Sr)-rich monazite at the above-mentioned sites is interpreted as a product of secondary and mainly hydrothermal alteration of the primary magmatic rocks, or its formation as a result of plagioclase breakdown during high-pressure metamorphism. The textural appearance of the Bacúch sulfatian–strontian monazite II also supports its secondary origin after the formation of primary, S,Sr-poor metamorphic monazite I. This presumably occurred during a younger, most likely Alpine tectonic and hydrothermal overprint of the parental rock. The younger hydrothermal veinlets with sulfide mineralization were most likely formed from H_2O–NaCl–KCl-type fluids over a temperature interval of 100–250°C and a salinity of 9–24 wt.% equiv. NaCl, as was previously determined in similar hydrothermal mineralization in the surrounding areas (Pršek & Chovan 2001). This mineralization is proposed to be a source of S for monazite II formation. The extremely low Th content in the monazite II also suggests growth under hydrothermal conditions (Schandl & Gorton 2004). Moreover, the enrichment in S coupled with the relative depletion in REE, may indicate a low pH, at least during the growth of monazite II (Fulignati *et al*. 1999).

The high Sr content correlated with the enrichment of Eu_2O_3, up to 2.7%, was interpreted as the breakdown of plagioclase under greenschist-facies conditions (Krenn *et al*. 2008). However, monazite II is Sr-enriched and depleted in Eu. The elevated Sr content together with Ca enrichment may be considered to be the result of hydrothermal leaching of Sr and Ca from Ca-bearing plagioclase, with simultaneous crystallization of albite during the Alpine overprint.

The chemical composition of the gadolinite–datolite-group minerals can be represented in the quadrilateral system by gadolinite ($R^{3+}Fe$), hingganite ($R^{3+}\square$), homilite ($Ca^{2+}Fe$) and datolite ($Ca^{2+}\square$) components (Fig. 7; Pezzotta *et al*. 1999). Hingganite can form by substituting in gadolinite the Fe vacancy through $\square(OH)_2Fe_{-1}O_{-2}$ (Burt 1989). This substitution trend is the most influential on the chemical composition of the Bacúch hingganite. Here, the hingganite has a very low Ca content (mostly <0.01 *apfu*), indicating a very small amount of the datolite component in the mineral. Hingganite-(Y) and gadolinite-(Y) mostly prefer REE with ionic radii closer to Y (Sm–Tb), which are mainly Dy and Gd (Demartin *et al*. 1993). However, our hingganite compositions show a distinctive enrichment in Nd (0.42 to 0.57 *apfu*) and, in some cases, Nd-dominant hingganite was detected (Table 3, Fig. 7). Unfortunately, the small size and the intimate intergrowths with associated minerals preclude structural analysis and definition as a new mineral. Consequently, the Nd contents of the Bacúch hingganite are the highest so far reported as naturally occurring, and they are significantly higher when compared to other occurrences of hingganite or gadolinite (*e.g.*, Demartin *et al*. 1993, Pezzotta *et al*. 1999, Miyawaki *et al*. 2007).

Gadolinite-group minerals and monazite from the veins and veinlets have been described in various metamorphic rocks in the Alps, and the surrounding rocks were interpreted to be a source of Be and REE (Demartin *et al*. 1991, 1993). Textural as well as compositional evidence indicates at least two main evolutionary stages of REE mineralization at Bacúch. (1) The origin of monazite I and xenotime is related to an older, probably Hercynian metamorphic event, together with the formation of magnetite. (2) The partial dissolution – re-precipitation of monazite I and xenotime and the formation of secondary S- and Sr-rich monazite II and Nd-rich hingganite occurred during the younger, Alpine (Cretaceous) tectonometamorphic and hydrothermal overprint of the Bacúch magnetite mineralization.

Acknowledgements

The authors thank Daniel Ozdín, Patrik Konečný, Ivan Holický, Radek Škoda and Petr Gadas for electron-microprobe assistance, and Ray Marshall for a review of the English content. Reviews by Michael L. Williams and Daniel E. Harlov greatly improved this paper. This work was supported by the Slovak Research and Development Agency under contract No. APVV–0557–06 and by research and equipment grants from the Slovak agency VEGA, grant number 1/1048/07. B. Budzyń is a fellow of the Foundation for Polish Science (START programme in 2008–2009).

References

ANTHONY, J., BIDEAUX, R., BLADH, K. & NICHOLS, M.C. (2000): *Handbook of Mineralogy*. IV. *Arsenates, Phosphates, Vanadates*. Mineral Data Publishing, Tucson, Arizona.

BEA, F. (1996): Residence of REE, Y, Th and U in granites and crustal protoliths; implications for the chemistry of crustal melts. *J. Petrol.* **37**, 521-552.

BIELY A., BEŇUŠKA, P., BEZÁK, V., BUJNOVSKÝ, A., HALOUZKA, R., IVANIČKA, J., KOHÚT, M., KLINEC, A., LUKÁČIK, E., MAGLAY, J., MIKO, O., PULEC, M., PUTIŠ, M. & VOZÁR, J. (1992): Geological map of the Nízke Tatry Mountains, 1: 50,000. State Geological Institute of Dionýz Štúr, Bratislava, Slovakia (in Slovak with English summary).

BORG, I.Y. & SMITH, D. K. (1975): A high pressure polymorph of $CaSO_4$. *Contrib. Mineral. Petrol.* **50**, 127-133.

BRADBURY, S.E. & WILLIAMS, Q. (2009): X-ray diffraction and infrared spectroscopy of monazite-structured $CaSO_4$ at high pressures: implications for shocked anhydrite. *J. Phys. Chem. Solids* **70**, 134-141.

BURT, D.M. (1989): Compositional and phase relations among rare earth element minerals. *In* Geochemistry and Mineralogy of Rare Earth Elements (B.R. Lipin & G.A. McKay, eds.). *Rev. Mineral.* **21**, 259-307.

CHAKHMOURADIAN, A. R. & MITCHELL, R. H. (1998): Lueshite, pyrochlore and monazite-(Ce) from apatite–dolomite carbonatite, Lesnaya Varaka complex, Kola Peninsula, Russia. *Mineral. Mag.* **62**, 769-782.

CHAKHMOURADIAN, A.R. & MITCHELL, R.H. (1999): Niobian ilmenite, hydroxylapatite and sulfatian monazite: alternative hosts for incompatible elements in calcite kimberlite from International'naya, Yakutia. *Can. Mineral.* **37**, 1177-1189.

CHOVAN, M., PRŠEK, J. & HURAIOVÁ, M. (2000): Mineralogy of the Bacúch ore occurrences. Unpubl. manuscript, Faculty of Natural Sciences, Bratislava, Slovakia (in Slovak).

CRESSEY, G., WALL, F. & CRESSEY, B.A. (1999): Differential REE uptake by sector growth of monazite. *Mineral. Mag.* **63**, 813-828.

CRICHTON, W.A., PARISE, J.B., ANTAO, S.M. & GRZECHNIK, A. (2005): Evidence for monazite-, barite- and $AgMnO_4$ (distorted barite)-type structures of $CaSO_4$ at high pressure and temperature. *Am. Mineral.* **90**, 22-27.

DALLMEYER, R.D., NEUBAUER, F. & PUTIŠ, M. (1993): $^{40}Ar/^{39}Ar$ mineral age controls for the Pre-Alpine and Alpine tectonic evolution of nappe complexes in the Western Carpathians. *PAEWCR Conf.* (*Stará Lesná, Slovakia*), *Excursion Guide*, 11-20.

DEMARTIN, F., PILATI, T., DIELLA, V., DONZELLI, S. & GRAMACCIOLI, C.M. (1991): Alpine monazite: further data. *Can. Mineral.* **29**, 61-67.

DEMARTIN, F., PILATI, T., DIELLA, V., GENTILE, P. & GRAMACCIOLI, C.M. (1993): A crystal-chemical investigation of Alpine gadolinite. *Can. Mineral.* **31**, 127-136.

DING XIAOSHI, BAI GE, YUAN ZHONGXIANG & SUN LUREN (1981): Yttroceberysite, a new Ce–Be-rich silicate. *Geol. Rev. China* **27**, 459-465 (in Chinese with English abstr.).

FÖRSTER, H.-J. (1998): The chemical composition of REE–Y–Th–U-rich accessory minerals in peraluminous granites of the Erzgebirge–Fichtelgebirge region, Germany. I. The monazite-(Ce) – brabantite solid solution series. *Am. Mineral.* **83**, 259-272.

FULIGNATI, P., GIONCADA, A. & SBRANA, A. (1999): Rare-earth element (REE) behaviour in the alteration facies of the active magmatic – hydrothermal system of Vulcano (Aeolian Islands, Italy). *J. Volcanol. Geotherm. Res.* **88**, 325-342.

GRAESER, S. & SCHWANDER, H. (1987): Gasparite-(Ce) and monazite-(Nd): two new minerals to the monazite group from the Alps. *Schweiz. Mineral. Petrogr. Mitt.* **67**, 103-113.

JERCINOVIĆ, M.J. & WILLIAMS, M.L. (2005): Analytical perils (and progress) in electron microprobe trace element analysis applied to geochronology: background acquisition, interferences, and beam irradiation effects. *Am. Mineral.* **90**, 526-246.

KONEČNÝ, P., SIMAN, P., HOLICKÝ, I., JANÁK, M. & KOLLÁROVÁ, V. (2004): Method of monazite dating by means of the microprobe. *Mineralia Slovaca* **36**, 225-235.

KORIKOVSKY, S.P., PUTIŠ, M. & PLAŠIENKA, D. (1997): Cretaceous low-grade metamorphism of the Veporic and North-Gemeric Zones: a result of collisional tectonics in the central Western Carpathians. *In* Geological Evolution of the Western Carpathians (P. Grecula, D. Hovorka & M. Putiš, eds.). *Mineralia Slovaca, Monograph*, 107-130.

KOTOV, A.B., MIKO, O., PUTIŠ, M., KORIKOVSKY, S.P., BEREZNAYA, N.G., KRÁĽ, J. & KRIST, E. (1996): U/Pb dating of zircons of postorogenic acid metavolcanics and metasubvolcanics: a record of Permian – Triassic taphrogeny of the West-Carpathian basement. *Geologica Carpathica* **47**, 73-79.

KRENN, E. & FINGER, F. (2004): Metamorphic formation of Sr-apatite and Sr-bearing monazite in a high-pressure rock from the Bohemian Massif. *Am. Mineral.* **89**, 1323-1329.

KRENN, E. & FINGER, F. (2007): Formation of monazite and rhabdophane at the expense of allanite during Alpine low temperature retrogression of metapelitic basement rocks from Crete, Greece: microprobe data and geochronological implications. *Lithos* **95**, 130-147.

KRENN, E., PUTZ, H., FINGER, F. & PAAR, W. (2008): Unusual monazite with high S, Sr, Eu and common Pb contents in ore bearing mylonites from the Schellgaden mining district, Austria. *Geophys. Res. Abstr.* **10**, EGU2008-A-11796.

KUKHARENKO, A.A., BULAKH, A.G. & BAKLANOVA, K.A. (1961): Sulfate-monazite from the Kola Peninsula carbonatites. *Zap. Vses. Mineral. Obshchest.* **90**, 373-381 (in Russ.).

KUKHARENKO, A.A., ORLOVA, M.P., BULAKH, A.G., BAGDASAROV, E.A., RIMSKAYA-KORSAKOVA, O.M., NEFEDOV, E.I., IL'INSKII, G.A., SERGEEV, A.S. & ABAKUMOVA, N.B. (1965): *The Caledonian Complex of Ultrabasic Alkaline Rocks and Carbonatites of the Kola Peninsula and Northern Karelia*. Nedra Press, Leningrad, Russia (in Russ.).

LISÝ, E. (1957): Final report up to the 1st of January 1957 at the Bacúch Fe part. Unpubl. manuscript, *Geofond*, Bratislava, Slovakia (in Slovak).

MASAU, M., ČERNÝ, P., COOPER, M.A., CHAPMAN, R. & GRICE, J.D. (2002): Monazite-(Sm), a new member of the monazite group from the Annie Claim #3 granitic pegmatite, southeastern Manitoba. *Can. Mineral.* **40**, 1649-1655.

MIYAWAKI, R., MATSUBARA, S., YOKOAMA, K. & OKAMOTO, A. (2007): Hingganite-(Ce) and hingganite-(Y) from Tahara, Hirukawa-mura, Gifu Prefecture, Japan: the description on a new mineral species of the Ce-analogue of hingganite-(Y) with a refinement of the crystal structure of hingganite-(Y). *J. Mineral. Petrol. Sci.* **102**, 1, 1-7.

MIYAWAKI, R., NAKAI, I., NAGASHIMA, K., OKAMOTO, A. & ISOBE, T. (1987): The first occurrences of hingganite, hellandite and wodginite in Japan. *Kobutsugaku Zasshi* **18**(1), 17-30 (in Japanese).

NI YUNXIANG, HUGHES, J.M. & MARIANO, A.N. (1995): Crystal chemistry of the monazite and xenotime structures. *Am. Mineral.*, **80**, 21-26.

ONDREJKA, M., UHER, P., PRŠEK, J. & OZDÍN, D. (2007): Arsenian monazite-(Ce) and xenotime-(Y), REE arsenates and carbonates from the Tisovec–Rejkovo rhyolite, Western Carpathians, Slovakia: composition and substitutions in the (REE,Y)XO_4 system (X = P, As, Si, Nb, S). *Lithos* **95**, 116-129.

PETRO, M. (1973): Mineral raw material at the sheet Polomka 1:25 000. Unpubl. manuscript, *Geofond*, Bratislava, Slovakia (in Slovak).

PEZZOTTA, F., DIELLA, V. & GUASTONI, A. (1999): Chemical and paragenetic data on gadolinite-group minerals from Baveno and Cuasso al Monte, Southern Alps, Italy. *Am. Mineral.* **84**, 782-789.

PRŠEK, J. & CHOVAN, M. (2001): Hydrothermal carbonate and sulphide mineralization in the Late Paleozoic phyllites (Bacúch, Nízke Tatry Mts.). *Geolines* **13**, 27-34.

SCHANDL, E.S. & GORTON, M.P. (2004): A textural and geochemical guide to the identification of hydrothermal monazite; criteria for selection of samples for dating epigenetic hydrothermal ore deposits. *Econ. Geol.* **99**, 1027-1035.

TAYLOR, S.R. & MCLENNAN, S.M. (1985): *The Continental Crust: Its Composition and Evolution*. Blackwell, Oxford, U.K.

ZYCH-HABEL, B., CHRUŚCIEL, A., & MICHALIK, M. (2007): Primary and secondary accessory minerals in the Strzeblów granite (Fore Sudetic block). *Mineralogia Polonica, Spec. Pap.* **31**, 323-326.

Received December 15, 2008, revised manuscript accepted January 5, 2010.